Type 3 innate lymphoid cells maintain intestinal epithelial stem cells after tissue damage

Patricia Aparicio-Domingo,[1]* Monica Romera-Hernandez,[1]* Julien J. Karrich,[1] Ferry Cornelissen,[1] Natalie Papazian,[1] Dicky J. Lindenbergh-Kortleve,[2] James A. Butler,[3] Louis Boon,[4] Mark C. Coles,[3] Janneke N. Samsom,[2] and Tom Cupedo[1]

[1]Department of Hematology and [2]Department of Pediatrics, Division of Gastroenterology and Nutrition, Erasmus University Medical Center, 3015 CN Rotterdam, Netherlands
[3]Centre for Immunology and Infection, Department of Biology and Hull York Medical School, University of York, York YO10 5DD, England, UK
[4]Bioceros, 3584 CM Utrecht, Netherlands

Disruption of the intestinal epithelial barrier allows bacterial translocation and predisposes to destructive inflammation. To ensure proper barrier composition, crypt–residing stem cells continuously proliferate and replenish all intestinal epithelial cells within days. As a consequence of this high mitotic activity, mucosal surfaces are frequently targeted by anticancer therapies, leading to dose–limiting side effects. The cellular mechanisms that control tissue protection and mucosal healing in response to intestinal damage remain poorly understood. Type 3 innate lymphoid cells (ILC3s) are regulators of homeostasis and tissue responses to infection at mucosal surfaces. We now demonstrate that ILC3s are required for epithelial activation and proliferation in response to small intestinal tissue damage induced by the chemotherapeutic agent methotrexate. Multiple subsets of ILC3s are activated after intestinal tissue damage, and in the absence of ILC3s, epithelial activation is lost, correlating with increased pathology and severe damage to the intestinal crypts. Using ILC3–deficient Lgr5 reporter mice, we show that maintenance of intestinal stem cells after damage is severely impaired in the absence of ILC3s or the ILC3 signature cytokine IL–22. These data unveil a novel function of ILC3s in limiting tissue damage by preserving tissue-specific stem cells.

CORRESPONDENCE
Tom Cupedo:
t.cupedo@erasmusmc.nl

Abbreviations used: IEC, intestinal epithelial cell; ILC3, type 3 innate lymphoid cell; ISC, intestinal stem cell; MTX, methotrexate; qPCR, quantitative PCR.

The intestinal epithelium combines efficient uptake of nutrients and water while providing a physical barrier between the intestinal microbiota and the body (Peterson and Artis, 2014). Damage sustained by intestinal epithelial cells (IECs) needs to be swiftly and efficiently repaired to prevent inappropriate immune responses to commensal bacteria. Intestinal damage is an early event in the development of both graft-versus-host disease (Reddy and Ferrara, 2003) and alimentary mucositis (Sonis, 2004) and a driver of bacterial translocation and T cell activation in inflammatory bowel disease (Salim and Söderholm, 2011).

A major pathway involved in the intestinal epithelial response to damage is the activation of Stat3, which is expressed along the crypt–villus axis of the intestinal epithelium (Grivennikov et al., 2009; Heneghan et al., 2013). Phosphorylated Stat3 translocates to the nucleus and activates genes involved in proliferation, survival, and mucosal defense (Bollrath et al., 2009; Pickert et al., 2009; Ernst et al., 2014). Mutations in *STAT3* have been identified as susceptibility factors for inflammatory bowel disease (Bollrath et al., 2009; Anderson et al., 2011; Demaria et al., 2012), and in mice, upon DSS-induced colitis, epithelial Stat3 is required for mucosal wound healing (Pickert et al., 2009).

Intestinal regeneration depends on the continuous differentiation of epithelial cells from crypt-residing intestinal stem cells (ISCs; Potten et al., 1978; Günther et al., 2013; Ritsma et al., 2014). Even though multiple intestinal progenitor

*P. Aparicio-Domingo and M. Romera-Hernandez contributed equally to this paper.

The Rockefeller University Press $30.00
J. Exp. Med. 2015 Vol. 212 No. 11   1783–1791
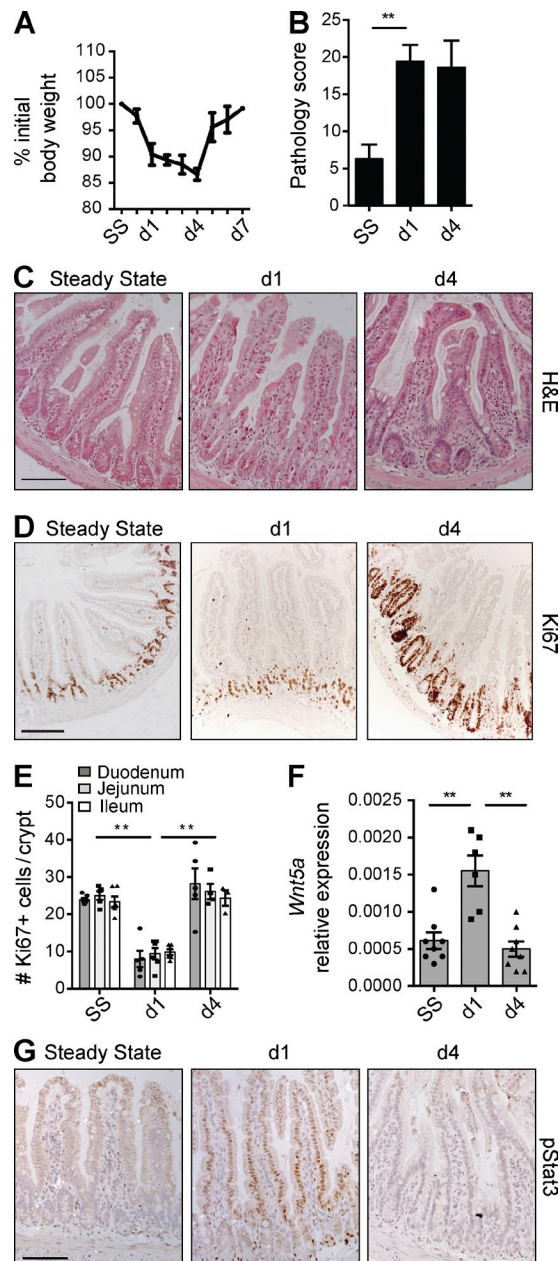www.jem.org/cgi/doi/10.1084/jem.20150318

1783

Figure 1. Epithelial responses to MTX. (A) Weight curve of WT mice treated with MTX. (B) MTX-induced pathology as described in Materials and methods. (C and D) Representative H&E staining (C) and immunostaining of Ki67 (D) in ileal sections at the indicated time points. (E) Number of KI67+ cells per crypt at the indicated time points. (F) Transcript analysis of *Wnt5a* in ileal tissues. (G) Representative immunostaining of pStat3 in ileal sections at the indicated time points. (A–C and G) Two to four independent experiments, *n* > 5 per time point. (D–F) Two independent experiments, *n* = 2–3 per time point. Mean ± SEM. **, P < 0.01. Bars, 50 µm.

cells have been described, the best-characterized populations are the Lgr5-expressing cells that reside at the crypt bottom, interspersed with Paneth cells. These stem cells have the ability to give rise to all IECs ex vivo (Sato et al., 2009). Similar

to its role in differentiated epithelial cells, Stat3 activation is also an important pathway for survival of intestinal epithelial stem cells (Matthews et al., 2011).

Type 3 innate lymphoid cells (ILC3s) are innate immune cells that reside in the lamina propria of both the small and large intestines and are involved in tissue homeostasis, early defense against enteric pathogens, and containment of microbiota (Spits and Cupedo, 2012; Artis and Spits, 2015). In the intestines, multiple ILC3 subsets exist, two of which can be distinguished by mutual exclusive expression of the natural cytotoxicity receptor NKp46 and the chemokine receptor CCR6 (Sawa et al., 2010; Reynders et al., 2011). Most Nkp46+ ILC3s are found dispersed throughout the lamina propria, a localization that depends on the expression of CXCR6 (Satoh-Takayama et al., 2014). In contrast, the majority of CCR6+ ILC3s are located in close proximity to the intestinal crypts in anatomically defined sites known as cryptopatches (Kanamori et al., 1996). Recent findings indicated that under inflammatory conditions, such as experimental graft-versus-host disease, ILC3s can interact with the epithelial stem cells in the crypts, protecting them from T cell–mediated killing (Hanash et al., 2012).

The well-known ability of ILC3s to condition the local microenvironment, the close proximity of ILC3s to intestinal crypts, and the ability of ILC3s to communicate with epithelial stem cells led us to hypothesize that ILC3s are involved in directing intestinal epithelial responses to tissue damage. Using the methotrexate (MTX) model of small intestinal damage, we now show that ILC3s are activated immediately after MTX administration, leading to a rapid activation of epithelial Stat3 and maintenance of ISCs. Our data reveal a novel function for ILC3s as organizers of the intestinal epithelial response to tissue damage through activation of epithelial cells and maintenance of ISCs and suggest that ILC3s might in future be therapeutically harnessed to prevent stem cell loss during chemotherapy.

RESULTS AND DISCUSSION

Damage–induced epithelial responses depend on Thy1+ cells

To study tissue damage responses in the small intestine, where most ILC3s reside, we exposed mice to MTX, an antimetabolite that inhibits folic acid metabolism and targets cells in S phase (Visentin et al., 2012). MTX application is a well-established, self-resolving model of small intestinal damage ideally suited to dissect epithelial responses to sterile insult (Verburg et al., 2002; de Koning et al., 2006; Frank et al., 2015). Upon MTX administration, mice lost weight until day 4, after which they fully recovered by day 7 (Fig. 1 A). This rapid weight loss correlated with intestinal pathology, which peaked as early as day 1 after the last MTX injection and subsequently stabilized at day 4 (Fig. 1 B) before recovering by day 7 (not depicted). Pathological examination of the small intestine showed villus flattening and crypt hyperplasia with an overall loss of epithelial architecture (Fig. 1 C).

To visualize damage responses by epithelial cells, we assessed the number of cycling crypt cells, a measure of regenerative
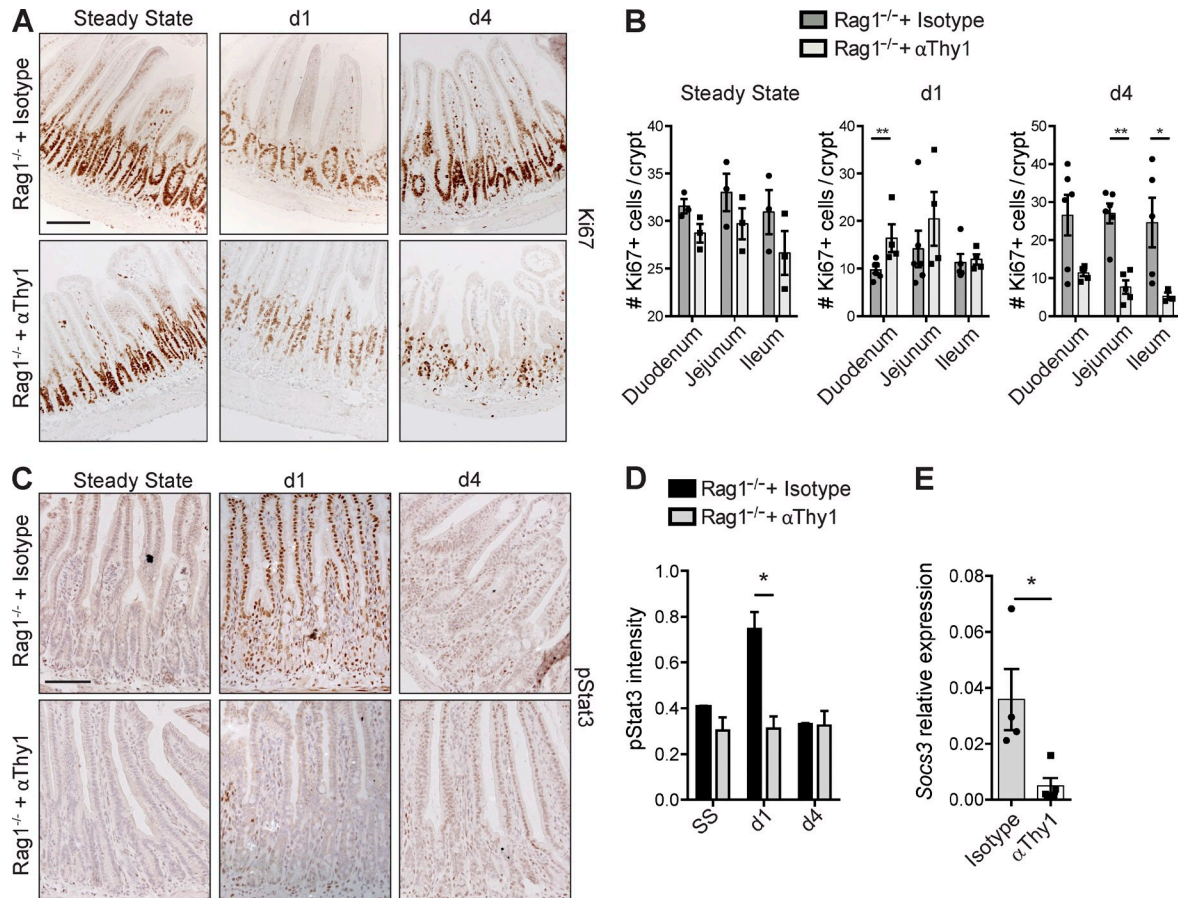
Figure 2. Epithelial responses to tissue damage depend on Thy1+ cells. (A and B) Representative immunostaining of Ki67 in isotype- and α-Thy1–treated Rag1$^{-/-}$ mice (A) and number of Ki67+ cells per crypt at the indicated time points (B). (C) Immunostaining of pStat3 in isotype- and α-Thy1–treated Rag1$^{-/-}$ mice. (D) pStat3 intensity in ileal sections at the indicated time points. (E) *Socs3* transcript levels relative to *Gapdh* from ileum at day 1 after MTX (two independent experiments, *n* = 2–5 per time point). Mean ± SEM. *, P < 0.05; **, P < 0.01. Bars, 50 µm.

capacity. Ki67+ crypt cells were reduced at day 1 but returned to baseline levels by day 4 (Fig. 1, D and E). Conversely, transcripts for the regeneration–associated Wnt family member Wnt5a (Miyoshi et al., 2012) were increased early after damage (Fig. 1 F). Phosphorylation of Stat3 in IECs plays a central role in mucosal wound healing (Ernst et al., 2014). Stat3 phosphorylation was induced early after MTX application, peaking at day 1 (Fig. 1 G). 4 d after the last MTX injection, the phosphorylation of Stat3 had returned to baseline (Fig. 1 G). These data show that MTX-induced small intestinal damage induces rapid and transient epithelial activation followed by regeneration.

Immediate MTX–induced pathology has been mainly attributed to direct effects on IECs, leading to epithelial cell–intrinsic responses to tissue damage (Verburg et al., 2002). To determine whether the restoration of cycling crypt cells and the phosphorylation of Stat3 are indeed epithelial cell intrinsic or whether immune cells are involved, we administered MTX to Rag1$^{-/-}$ mice that lack adaptive immunity and to Rag1$^{-/-}$ mice pretreated with Thy1-depleting antibodies to eradicate innate immune cell subsets. Rag1$^{-/-}$ mice treated

with isotype control antibodies showed normal restoration of the proliferative crypt compartment at day 4 (Fig. 2, A and B) and normal phosphorylation of Stat3 at day 1 after MTX (Fig. 2 C), confirming that adaptive immune cells are dispensable for these epithelial responses. In contrast, depletion of Thy1+ cells in Rag1$^{-/-}$ mice strongly reduced the recovery of cycling cells at day 4 (Fig. 2, A and B) and impaired Stat3 phosphorylation in IECs in response to tissue damage (Fig. 2 C). To validate the reduced Stat3 phosphorylation, we quantified the intensity of pStat3 staining on tissue sections using semi-automated analysis and found a significant reduction in pStat3 intensity at day 1 after the last MTX administration (Fig. 2 D). In addition, transcript analysis of total ileum revealed a reduction in levels of the Stat3 target gene *Socs3*, indicative of reduced Stat3 signaling (Fig. 2 E). Of note, pStat3-positive hematopoietic cells were found in the lamina propria of both control Rag1$^{-/-}$ and Thy1-depleted Rag1$^{-/-}$ mice (Fig. 2 C), suggesting differential regulation of Stat3 activation in epithelial and hematopoietic cells. In conclusion, these experiments establish that restoration of the proliferating crypt cell compartment and epithelial phosphorylation of Stat3 after tissue
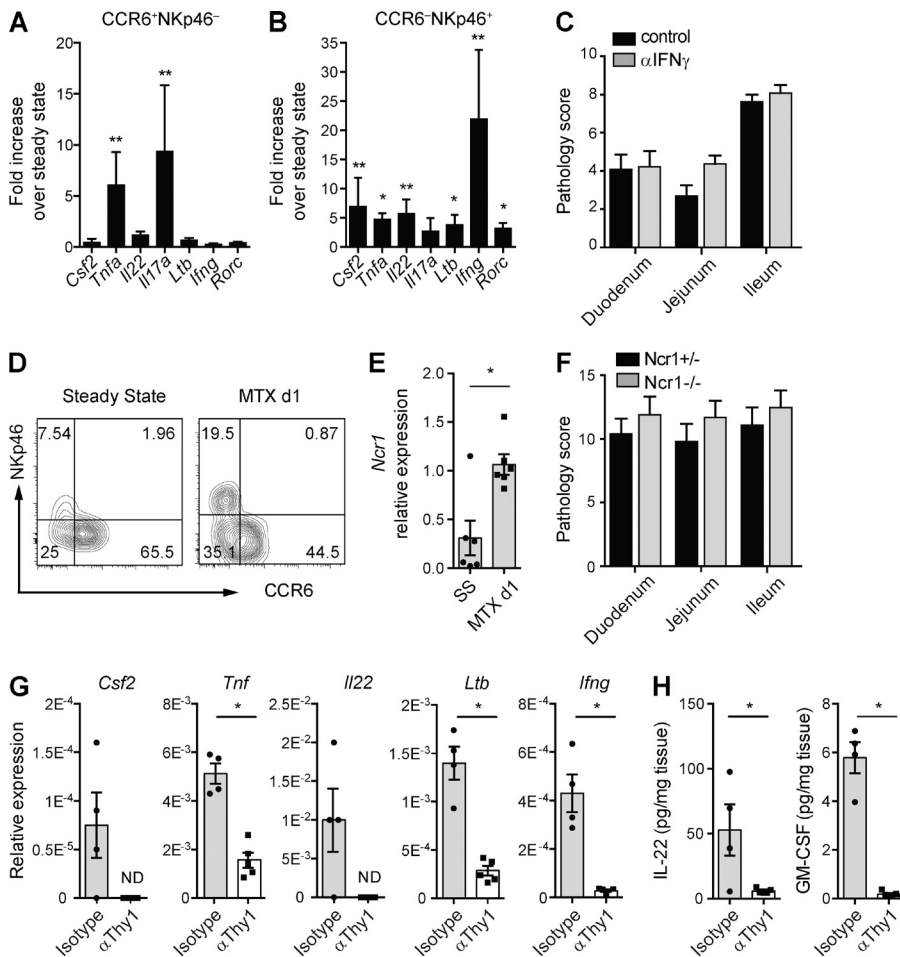
Figure 3. ILC3s are activated upon MTX–induced damage. (A and B) Fold induction of the indicated transcripts relative to steady state of lamina propria CCR6+NKp46− ILC3s (A) and CCR6−NKp46+ ILC3s (B) at day 1 after MTX. (C) Pathology score at day 4 after MTX of intestines of Rag1−/− mice treated with neutralizing IFNγ or isotype control antibodies. (D) Representative flow cytometry plot of NKp46 and CCR6 expression on lamina propria ILC3s at steady state and day 1 after MTX. (E) Transcript levels of *Ncr1* relative to *Gapdh* from sorted CCR6−NKp46+ ILC3s. (F) Pathology score at day 4 after MTX of intestines of Ncr1+/− or Ncr1−/− mice. (G) Transcriptional analyses of the indicated genes relative to *Gapdh* from ileum of isotype control or Thy1–depleted Rag1−/− mice at day 1 after MTX. (H) Protein levels of IL-22 and GM-CSF after overnight ileal explant cultures isolated at day 1 after MTX. (A, B, D, and E) Four to six independent experiments, *n* = 5–7 per time point. (C and F) Two independent experiments, *n* = 2–4 per group. (G and H) Two independent experiments, *n* = 2–3 per group. Mean ± SEM. *, P < 0.05; **, P < 0.01. ND, not detected.

damage are not epithelial cell–intrinsic responses but require the presence of Thy1+ cells.

ILC3s are activated in response to intestinal tissue damage

The finding that phosphorylation of epithelial Stat3 depends on Thy1+ cells led us to hypothesize that Thy1+ ILC3s are involved in the intestinal response to MTX-induced tissue damage. To determine whether ILC3s are activated in response to intestinal damage, CCR6+ and NKp46+ lamina propria ILC3s were analyzed for expression of activation-associated transcripts at 1 d after the last MTX injection (Fig. 3 A and B). Compared with homeostasis, CCR6+ ILC3s maintained transcription of *Ltb*, *Rorc*, *Ifng*, *Il22*, and *Csf2* but showed increased transcription of *Tnf* and *Il17a* (Fig. 3 A). NKp46+ ILC3s significantly increased transcription of *Ltb*, *Rorc*, *Il22*, *Ifng*, *Csf2*, and *Tnf* (Fig. 3 B). These data show that in response to intestinal tissue damage, both NKp46+ and CCR6+ ILC3s are activated, albeit in a differential manner. IFNγ-secreting ILC3s have been implicated in intestinal pathology (Klose et al., 2013), and we therefore assessed the contribution of this ILC3-derived cytokine to MTX-induced damage by neutralizing IFNγ in Rag1−/− mice. After exposure to MTX, intestinal

pathology was similar in Rag1−/− mice treated with either neutralizing IFNγ antibodies or isotype controls, suggesting that IFNγ is not critical for pathology in this model (Fig. 3 C). In line with the activation of ILC3s at the cytokine level, we also noted that expression of NKp46 was increased on ILC3s at day 1 after insult. This increased expression was apparent both at the protein (Fig. 3 D) and transcript level (Fig. 3 E). We next exposed Ncr1−/− and littermate controls to MTX to determine whether absence of Nkp46 influences MTX-induced pathology. However, the overall pathology in Ncr1−/− mice did not differ from the Ncr1+/− littermate controls, arguing against an essential role of NKp46 in response to MTX (Fig. 3 F). To confirm the transcription of the ILC3 activation–associated cytokines in an in vivo setting, we analyzed the intestines of Rag1−/− mice in the presence or absence of Thy1+ cells. Transcript analysis of total ileum or protein analysis after overnight ileal explant cultures clearly showed that the presence of Thy1+ cells was essential for generation of transcripts for *Csf2*, *Tnf*, *Il22*, *Ltb*, and *Ifng* (Fig. 3 G), as well as protein for both IL-22 and GM-CSF (Fig. 3 H) in response to tissue damage. These experiments unveil the rapid activation of ILC3 subsets in response to intestinal tissue damage.
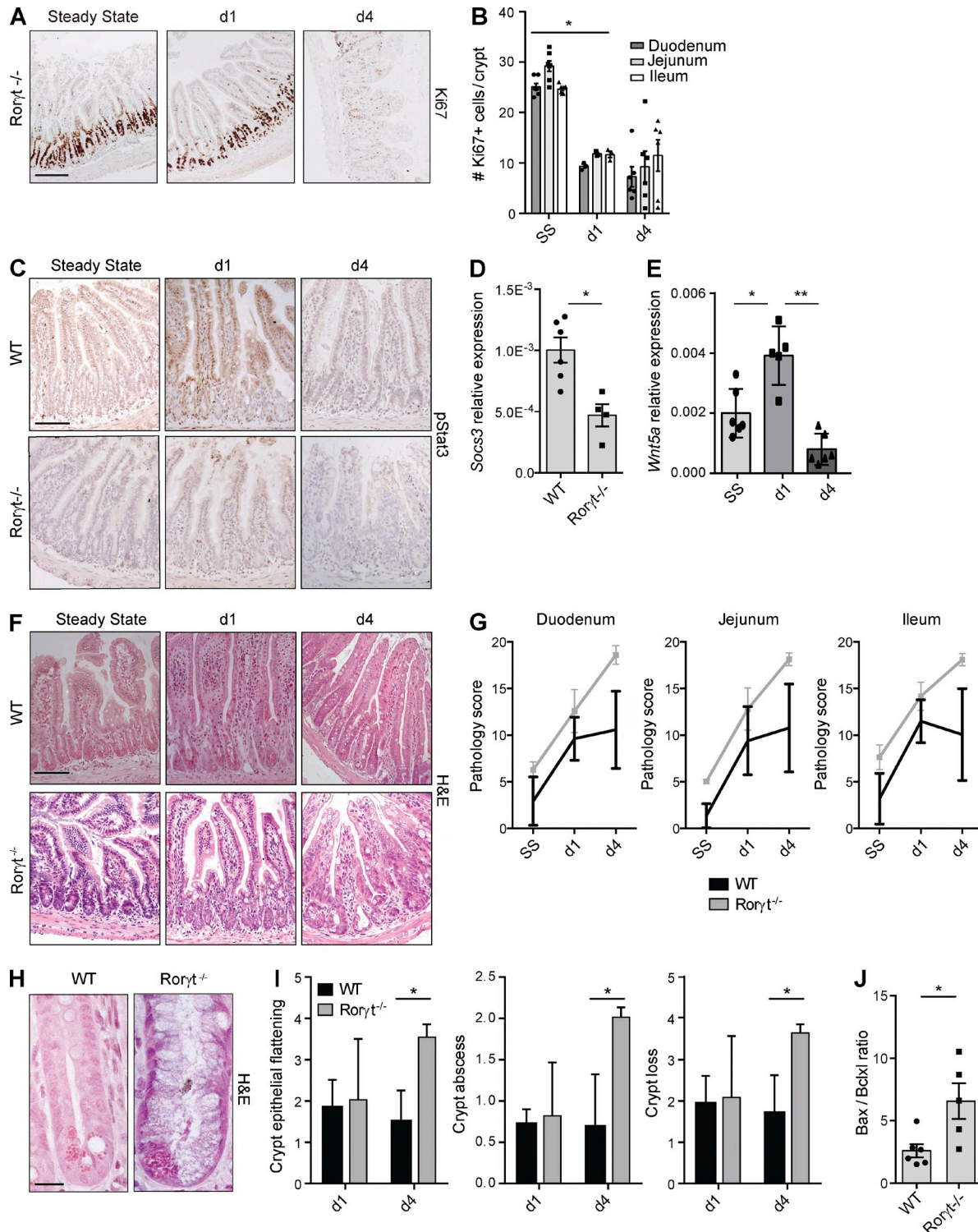
Figure 4. Absence of Rorγt augments crypt damage after MTX. (A) Ki67 in ileum sections of Rorγt$^{-/-}$ mice at the indicated time points. (B) Number of Ki67$^+$ cells in crypts of Rorγt$^{-/-}$ mice at the indicated time points. (C) pStat3 in ileum sections from WT and Rorγt$^{-/-}$ mice at the indicated time points. (D) *Socs3* transcripts relative to *Gapdh* from ileum of WT and Rorγt$^{-/-}$ mice at day 1 after MTX. (E) *Wnt5a* transcripts from ileum of Rorγt$^{-/-}$ mice at the indicated time points. (F) Representative H&E staining of ileal sections at the indicated time points. (G) MTX-induced small intestinal damage in WT and Rorγt$^{-/-}$ mice as specified in Materials and methods. (H) Representative high-power magnification of ileal crypts of WT and Rorγt$^{-/-}$ mice 4 d after MTX. (I) Crypt damage in WT and Rorγt$^{-/-}$ mice at days 1 and 4. (J) Ratio between *bax* and *bcl2l1* transcript levels in ileum of WT and Rorγt$^{-/-}$ mice at day 1 after MTX. (A and B) Two independent experiments, n = 3–4 per group. (C, D, and F–I) Two to four independent experiments, n = 2–5 per group. (E and J) Two independent experiments, n = 2–3 per group. Mean ± SEM. *, P < 0.05; **, P < 0.01. Bars: 50 µm (A, C, and F); 10 µm (H).

ILC3 deficiency aggravates MTX–induced damage

Depletion of Thy1^{+} cells diminished regeneration of crypt cells and activation of epithelial Stat3 in response to MTX, and ILC3s were activated early after tissue damage. However, because Thy1 antibodies do not specifically target ILC3s, we next exposed ILC3-deficient Rorγt^{−/−} mice to MTX to confirm that ILC3s are responsible for the observed damage-associated epithelial responses. Rorγt^{−/−} mice showed impaired recovery of the cycling crypt compartment at day 4 after MTX (Fig. 4, A and B), and IECs in Rorγt^{−/−} mice did not show phosphorylation of Stat3 in response to tissue damage (Fig. 4 C). Consequently, Stat3 signaling was reduced as indicated by lower levels of *Socs3* transcripts (Fig. 4 D). In contrast, induction of *Wnt5a* transcription was independent of ILC3s and occurred normally in Rorγt^{−/−} mice (Fig. 4 E).

Histological analysis of the small intestines of MTX-exposed Rorγt^{−/−} mice revealed a slight increase in overall pathology at day 4 after MTX (Fig. 4 F). The differences in overall pathology between WT and Rorγt^{−/−} mice did not reach statistical significance, even though there seemed to be a trend toward increased pathology in Rorγt^{−/−} mice at day 4 (Fig. 4 G).

To understand this trend, we performed differential pathology scoring on intestinal villus and crypt compartments. This revealed a significant increase in the damage sustained by the small intestinal crypts in Rorγt^{−/−} mice compared with control mice (Fig. 4 H). The extent of crypt epithelial flattening, the presence of crypt abscesses, and the eventual loss of crypts were all significantly increased in the absence of Rorγt (Fig. 4 I). Survival of epithelial cells in response to tissue damage is regulated by the balance between several pro- and antiapoptotic molecules (Vereecke et al., 2011). To assess whether this balance was shifted in the absence of Rorγt, we determined transcript levels of the proapoptotic gene *Bax* and the antiapoptotic gene *Bcl2l1* (BclXL) in ileum (Fig. 3 G). In Rorγt^{−/−} mice, 1 d after MTX, the *Bax/Bcl2l1* ratio was significantly increased, indicating a shift toward a more proapoptotic program in the absence of ILC3s. Combined, these data suggest that the absence of Rorγt[+] ILC3s augments tissue damage to the stem cell–containing intestinal crypts in response to MTX.

ILC3s preserve ISCs after tissue damage

A prerequisite for epithelial regeneration is the presence of crypt-residing ISCs (Potten, 1990). Because Rorγt^{−/−} mice exposed to MTX had increased crypt pathology and reduced crypt proliferation, we investigated the fate of Lgr5^{+} ISCs in response to MTX. To determine whether Lgr5^{+} ISCs are sensitive to MTX, we exposed Lgr5-GFP reporter mice to MTX and assessed the percentage of GFP^{+} cells in purified crypts of duodenum, jejunum, and ileum at several time points after treatment (Fig. 5 A). Lgr5^{+} ISC numbers declined directly after treatment, indicating that ISCs were targeted by MTX. Stem cell recovery started after day 4 and numbers

normalized by day 6 (Fig. 5 A). To investigate the role of Rorγt–expressing ILC3s in epithelial stem cell maintenance, we generated radiation bone marrow chimeras by transferring either WT or Rorγt-deficient bone marrow into lethally irradiated Lgr5-GFP recipient mice. To eliminate host-derived radioresistant ILC3s, both groups were treated with depleting α-Thy1 antibodies. Such Rorγt^{−/−}-Lgr5-GFP chimeric mice provide a model to study GFP-labeled Lgr5^{+} ISCs in the absence of Rorγt^{+} hematopoietic cells. In response to MTX, Rorγt^{−/−}-Lgr5-GFP chimeric mice developed increased intestinal pathology compared with WT chimeric mice (Fig. 5, B and C), as characterized by crypt epithelial flattening, crypt abscesses, and crypt loss (Fig. 5 D), resembling the pathology in Rorγt-deficient mice. To determine the effect of absence of Rorγt[+] lymphocytes on ISCs, we purified small intestinal crypts from Rorγt-sufficient and -deficient chimeric mice. At steady state, the percentages of Lgr5-GFP^{+} cells did not significantly differ between both groups (Fig. 5 E). At day 4 after MTX, flow cytometric analyses revealed a significant reduction in the percentage of Lgr5-GFP[+] ISCs within the EpCAM-1^{+} crypt epithelial cell fraction (Fig. 5 F). This reduction in Lgr5^{+} ISCs occurred along the entire length of the small intestine. In duodenum, jejunum, and ileum Lgr5^{+} ISCs were reduced by 68% (68.3 ± 3.1%), 71% (71.2 ± 1.4%), and 52% (52.1 ± 8.1%), respectively (Fig. 5 G), highlighting the importance of Rorγt[+] ILC3s as guardians of ISCs after damage.

IL-22 is an ILC3 signature cytokine involved in communication between ILC3s and crypt epithelial cells (Hanash et al., 2012) and is transcribed after MTX–induced damage. To determine whether IL-22 mechanistically links ILC3s to stem cell maintenance after damage, we used antibodies to neutralize this cytokine during MTX treatment. IL-22 blockade led to a significant loss of stem cell maintenance in the duodenum, whereas ISC numbers in jejunum and ileum were less affected (Fig. 5, H and I). These data indicate that IL-22 is one of the factors involved in stem cell maintenance after tissue damage.

Collectively, our findings reveal that ILC3s preserve organ-specific stem cells in response to tissue insult. MTX application evokes a rapid and transient activation of epithelial Stat3, followed by epithelial regeneration in a Thy1^{+}Rorγt[+] cell–dependent manner. Multiple subsets of ILC3s respond to intestinal tissue damage, and absence of ILC3s aggravates pathology in intestinal crypts. Importantly, we could show that the maintenance of ISCs after cytotoxic therapy is regulated by ILC3s and that, mechanistically, IL-22 is one of the effector molecules involved. Our findings thus highlight a previously unappreciated feature of ILC3s in coordinating epithelial responses to tissue damage in the small intestine. Their location in close proximity to the crypts and their resistance to chemo- and radiotherapy-induced cell death put ILC3s in the ideal position to minimize tissue damage after cytotoxic insult, and controlling ILC3 responses might hold the key to designing future therapeutic strategies aimed at minimizing intestinal damage in patients undergoing anticancer therapies.
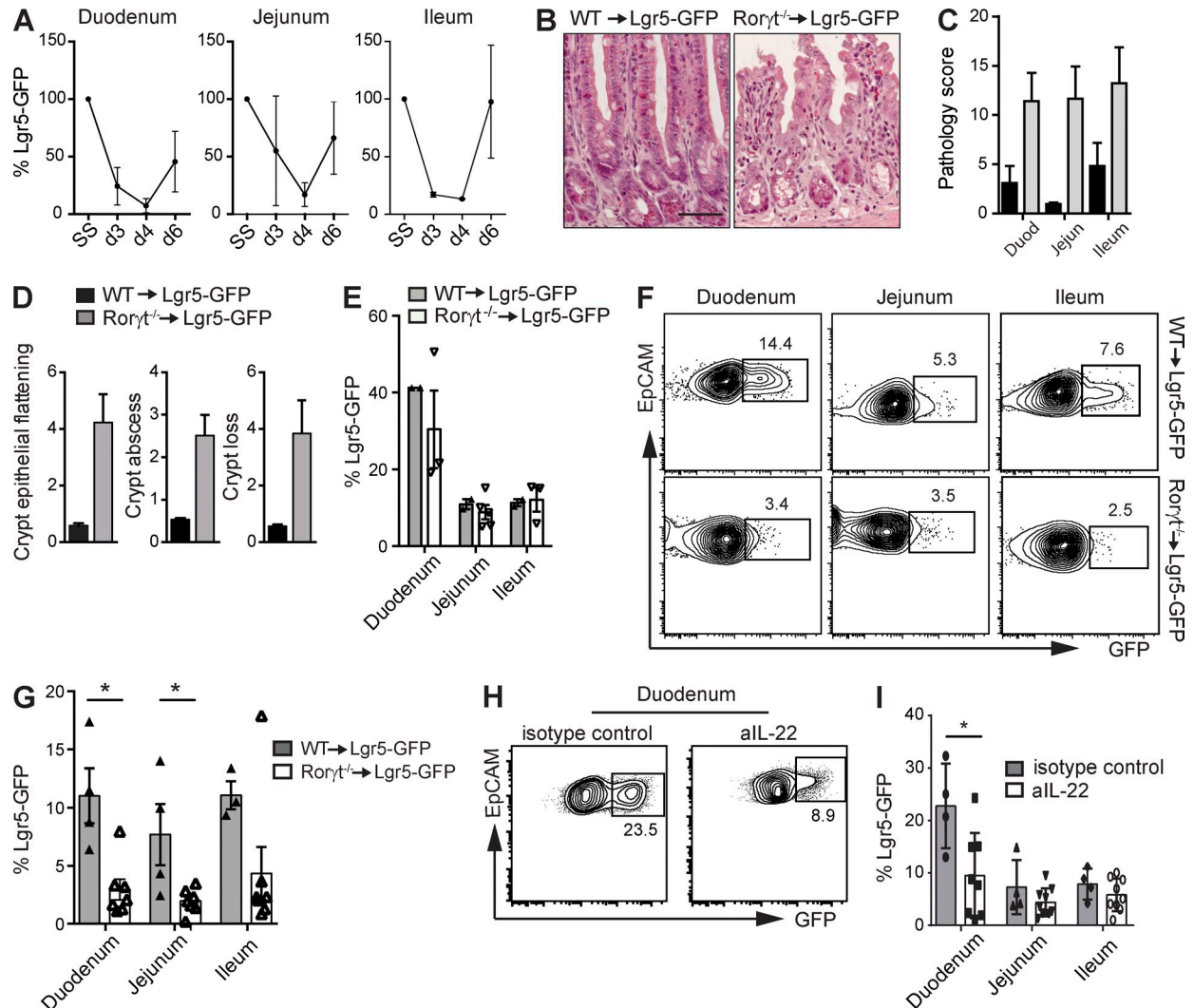
Figure 5. ILC3s preserve ISCs after MTX–induced damage. (A) Percentage of GFP+ stem cells within EpCAM1+ cells from purified intestinal crypts at the indicated time points. (B) Representative H&E staining of ileal sections of WT and Rorγt−/− chimeras at day 4 after MTX. (C) Small intestinal damage in WT (black bars) and Rorγt−/− (gray bars) chimeras at day 4 after MTX as described in Materials and methods. (D) Crypt pathology score. (E) Frequency of GFP+ cells from WT and Rorγt−/− chimeras at homeostasis. (F) Representative plots of purified crypts of WT and Rorγt−/− chimeras at day 4 after MTX. Numbers adjacent to outlined areas indicate percentage of EpCAM+Lgr5-GFP+ cells. (G) Frequency of GFP+ cells from WT and Rorγt−/− chimeras at day 4 after MTX. (H) Representative plots of purified duodenal crypts at day 4 after MTX of Lgr5-GFP mice treated with aIL-22 or control antibodies. (I) Frequency of GFP+ cells at day 4 after MTX from Lgr5-GFP mice treated with aIL-22 or control antibodies. (A) Two independent experiments, n = 2 per group. (B–D, F, and G) Two independent experiments with two to four mice per group. (E) Two independent experiments, WT: n = 1 per group, KO: n = 1–3 per group. (H and I) Two independent experiments with two to five mice per group. Mean ± SEM. *, P < 0.05. Bar, 50 µm.

MATERIALS AND METHODS

Mice. C57BL/6, Rorγt−/−, Rag1−/−, Ncr1−/− (a gift from O. Mandelboim, Hebrew University of Jerusalem, Jerusalem, Israel; Gazit et al., 2006), and Lgr5-eGFP mice were bred in the animal facility of the Erasmus University Medical Center Rotterdam. Animal experiments were approved by the Animal Ethics Committee of the ErasmusMC and performed in accordance with institutional guidelines. Age- and gender-matched littermates were used whenever possible.

Thy1+ cells were depleted using α-Thy1 antibodies (clone YTS154; provided by H. Waldmann, University of Cambridge, Cambridge, England, UK) or isotype controls (a-phytochrome AFRC MAC5.1). Antibodies were diluted in saline and mice were injected i.p. with 200 µg every other day for 2 wk.

Monoclonal antibodies. Monoclonal antibodies used were EpCAM-1 (G8.8; BioLegend); CD45 (30F11; Invitrogen); Lin-biotin (eBioscience); CD19 (1D3), CD3 (145-2C11), CD11c (N418), CD11b (M1/70), Gr1 (RB6-8C5), and Streptavidin (BioLegend); NK1.1 (PK136; eBioscience); CD127 (A7R34; eBioscience); CD117 (2B8; BD); NKp46 (2941.4; eBioscience); and CCR6 (29-2L17; BioLegend).

MTX. 8–12-wk-old mice were injected i.p. with 120 mg/kg MTX (PCH) at day −1 and with 60 mg/kg at day 0. Body weight was monitored daily, and tissues were collected at days 1 and 4 after the last MTX injection.

Cytokine neutralization. 150 µg anti–IL-22 antibody (8E11; gift from W. Ouyang, Genentech, South San Francisco, CA) or mouse IgG1 isotype

control (MOPC-21; Bio X Cell) was administered i.p. to Lgr5-eGFP mice every 2 d, starting 5 d before the first MTX dose, until day 2 after the last MTX dose. Rag1$^{-/-}$ mice were treated with 1 mg anti-IFNγ (XMG 1.2) or IgG1 isotype control (GL113) together with the first dose of MTX at day −1 and with 0.5 mg on days 0 and 1.

Radiation chimeras. 8-wk-old Lgr5-GFP mice were irradiated at 9 Gy and subsequently reconstituted by i.v. injection of 1–2 × 10^6 bone marrow cells from either WT or Rorγt$^{-/-}$ mice. Mice were under antibiotic water for 2 wk after bone marrow transplantation. To eliminate radioresistant ILC3s, 2 wk after reconstitution, Lgr5-GFP chimeras received five i.p. injections with 200 μg α-Thy1 antibody (YTS154; provided by H. Waldmann) during 2 wk. 4 wk after Thy1 depletion, Lgr5-GFP chimeras were exposed to MTX.

Crypt isolation. Isolation of intestinal crypts was performed as previously described (Sato et al., 2009). In brief, isolated small intestines were opened longitudinally and washed with cold PBS. Tissues were cut into 5-mm pieces and subsequently washed by mechanical pipetting with cold PBS until supernatant was clear. Tissues were incubated with 2 mM EDTA in PBS at 4°C for 30 min. Tissues were then washed several times with cold PBS and suspended by vigorous pipetting. Crypt-enriched sediments were passed through a 70-μm cell strainer and centrifuged at 600 rpm for 3 min to separate the crypts from single cells. Crypts were incubated with 1 ml TrypLE Express (Gibco) at 37°C for 10–15 min until crypt dissociation was observed. Single cell suspensions were stained with conjugated antibodies and analyzed for the expression of GFP by flow cytometry (FACSCanto II; BD).

Histology. 5-mm small intestinal tissue pieces were fixed in 4% PFA and embedded in paraffin. 4-μm sections were deparaffinized and stained with hematoxylin (Vector Laboratories) and eosin (Sigma-Aldrich; H&E). For Ki67 and pStat3 detection, endogenous peroxidases were blocked and antigen retrieval was achieved by microwave treatment in 10 mM citrate buffer, pH 6.0. Before staining, Fc receptors were blocked in blocking solution (blocking endogenous peroxidase: 1% periodic acid in deionized water for 20 min; blocking Fc receptors: 10% normal mouse serum, 10 mM Tris buffer, 5 mM EDTA, 0.15 M NaCl, 0.25% gelatin, and 0.05% Tween-20, pH 8.0). Tissue sections were incubated overnight at 4°C with rat Ki67 monoclonal antibody (MIB-5; Dako) or rabbit pStat3 antibody (D3A7; Cell Signaling Technology). Immunoreactions were detected using biotinylated donkey anti–rat and goat anti–rabbit (Vector Laboratories) and incubated with the VECTASTAIN ABC Elite kit (Vector Laboratories) and 3,3′-diaminobenzidine tetrahydrochloride (Sigma-Aldrich). Sections were counterstained with hematoxylin.

Both the analysis of pathology and Ki67$^+$ cells was performed blinded by at least two independent analysts. Pathology score was obtained as previously described (de Koning et al., 2006), and Ki67-expressing cells were counted in 5–12 crypts per section. Measurement of pStat3 intensity in IECs from sections was determined using HistoQuest software (TissueGnostics).

Explant cultures. Isolated small intestine was opened longitudinally and cleaned with cold PBS. A piece of 1-cm length was cultured in RPMI with 10% FCSi and 1% P/S at 37°C for 24 h. Protein content of supernatants was determined by enzyme-linked immunosorbent assay (eBioscience), and absorbance was measured at 450 nm using Victor X4 (PerkinElmer). Protein content of the supernatants was calculated relative to tissue weight.

Isolation of lamina propria lymphocytes. Isolated small intestine was opened longitudinally and washed with cold HBSS containing 15 mM Hepes, pH 7.2. Tissues were cut in 1-cm pieces and incubated in HBSS buffer containing 10% FBS, 15 mM Hepes, 5 mM EDTA, and 1 mM DTT, pH 7.2, at 37°C two times for 20 min to remove epithelium and intraepithelial lymphocytes. The tissues were digested with 100 U/ml Collagenase VIII (Sigma-Aldrich) in RPMI containing 10% FBS, 15 mM Hepes, 100 U/ml P/S, and 1 mM DTT, pH 7.2, at 37°C in a shaker two

times for 1 h. Supernatants were passed through a 70-μm cell strainer and washed in cold HBSS. Pellets were suspended in 90% Percoll, overlaid with 40% Percoll, and centrifuged at 1,800 rpm for 20 min to allow separation of mononuclear cells by density gradient. Interphase was washed and stained with conjugated antibodies. Lamina propria lymphocytes were analyzed by flow cytometry (FACSAria III; BD), and ILC3s were sorted as CD45$^+$Lin$^-$NK1.1$^-$CD127$^+$CD117$^+$CCR6$^{+/-}$NKp46$^{+/-}$ (see Fig. S1 for full gating strategy).

Transcript analysis. RNA was extracted using the NucleoSpin RNA XS kit (MACHERY-NAGEL). RNA from sorted cells was amplified according to the manufacturer's protocol (Ovation PicoSL WTA System V2; NuGen). For quantitative PCR (qPCR), a Neviti Thermal Cycler (Applied Biosystems) and DyNAmo Flash SYBR Green qPCR kit (Finnzymes) were used, with the addition of MgCl$_2$ to a final concentration of 4 mM. All reactions were performed in duplicate and are normalized to the expression of Gapdh. Relative expression was calculated by the cycling threshold (CT) method as $2^{-\Delta CT}$. The primer sequences can be found in Table S1.

Statistical analysis. Samples were analyzed using unpaired Mann–Whitney test. P-values <0.05 were considered significant. Data are shown as mean ± SEM.

Online supplemental information. Fig. S1 shows the gating strategy for lamina propria ILC3s. Table S1 lists the primer sequences used for qPCR. Online supplemental material is available at http://www.jem.org/cgi/content/full/jem.20150318/DC1.

REFERENCES

Anderson, C.A., G. Boucher, C.W. Lees, A. Franke, M. D'Amato, K.D. Taylor, J.C. Lee, P. Goyette, M. Imielinski, A. Latiano, et al. 2011. Meta-analysis identifies 29 additional ulcerative colitis risk loci, increasing the number of confirmed associations to 47. *Nat. Genet.* 43:246–252. http://dx.doi.org/10.1038/ng.764

Artis, D., and H. Spits. 2015. The biology of innate lymphoid cells. *Nature.* 517:293–301. http://dx.doi.org/10.1038/nature14189

Bollrath, J., T.J. Phesse, V.A. von Burstin, T. Putoczki, M. Bennecke, T. Bateman, T. Nebelsiek, T. Lundgren-May, O. Canli, S. Schwitalla, et al. 2009. gp130-mediated Stat3 activation in enterocytes regulates cell survival and cell-cycle progression during colitis-associated tumorigenesis. *Cancer Cell.* 15:91–102. http://dx.doi.org/10.1016/j.ccr.2009.01.002

de Koning, B.A., J.M. van Dieren, D.J. Lindenbergh-Kortleve, M. van der Sluis, T. Matsumoto, K. Yamaguchi, A.W. Einerhand, J.N. Samsom, R. Pieters, and E.E. Nieuwenhuis. 2006. Contributions of mucosal immune cells to methotrexate-induced mucositis. *Int. Immunol.* 18:941–949. http://dx.doi.org/10.1093/intimm/dxl030

Demaria, M., S. Misale, C. Giorgi, V. Miano, A. Camporeale, J. Campisi, P. Pinton, and V. Poli. 2012. STAT3 can serve as a hit in the process of malignant transformation of primary cells. *Cell Death Differ.* 19:1390–1397. http://dx.doi.org/10.1038/cdd.2012.20

Ernst, M., S. Thiem, P.M. Nguyen, M. Eissmann, and T.L. Putoczki. 2014. Epithelial gp130/Stat3 functions: an intestinal signaling node in health and disease. *Semin. Immunol.* 26:29–37. http://dx.doi.org/10.1016/j.smim.2013.12.006

ILC3s control intestinal damage responses | Aparicio-Domingo et al.

Frank, M., E.M. Hennenberg, A. Eyking, M. Rünzi, G. Gerken, P. Scott, J. Parkhill, A.W. Walker, and E. Cario. 2015. TLR signaling modulates side effects of anticancer therapy in the small intestine. *J. Immunol.* 194:1983–1995. http://dx.doi.org/10.4049/jimmunol.1402481

Gazit, R., R. Gruda, M. Elboim, T.I. Arnon, G. Katz, H. Achdout, J. Hanna, U. Qimron, G. Landau, E. Greenbaum, et al. 2006. Lethal influenza infection in the absence of the natural killer cell receptor gene *Ncr1*. *Nat. Immunol.* 7:517–523. http://dx.doi.org/10.1038/ni1322

Grivennikov, S., E. Karin, J. Terzic, D. Mucida, G.Y. Yu, S. Vallabhapurapu, J. Scheller, S. Rose-John, H. Cheroutre, L. Eckmann, and M. Karin. 2009. IL-6 and Stat3 are required for survival of intestinal epithelial cells and development of colitis-associated cancer. *Cancer Cell.* 15:103–113. http://dx.doi.org/10.1016/j.ccr.2009.01.001

Günther, C., H. Neumann, M.F. Neurath, and C. Becker. 2013. Apoptosis, necrosis and necroptosis: cell death regulation in the intestinal epithelium. *Gut.* 62:1062–1071. http://dx.doi.org/10.1136/gutjnl-2011-301364

Hanash, A.M., J.A. Dudakov, G. Hua, M.H. O'Connor, L.F. Young, N.V. Singer, M.L. West, R.R. Jenq, A.M. Holland, L.W. Kappel, et al. 2012. Interleukin-22 protects intestinal stem cells from immune-mediated tissue damage and regulates sensitivity to graft versus host disease. *Immunity.* 37:339–350. http://dx.doi.org/10.1016/j.immuni.2012.05.028

Heneghan, A.F., J.F. Pierre, and K.A. Kudsk. 2013. JAK-STAT and intestinal mucosal immunology. *JAK-STAT.* 2:e25530. http://dx.doi.org/10.4161/jkst.25530

Kanamori, Y., K. Ishimaru, M. Nanno, K. Maki, K. Ikuta, H. Nariuchi, and H. Ishikawa. 1996. Identification of novel lymphoid tissues in murine intestinal mucosa where clusters of c-kit+ IL-7R+ Thy1+ lympho-hemopoietic progenitors develop. *J. Exp. Med.* 184:1449–1459. http://dx.doi.org/10.1084/jem.184.4.1449

Klose, C.S., E.A. Kiss, V. Schwierzeck, K. Ebert, T. Hoyler, Y. d'Hargues, N. Göppert, A.L. Croxford, A. Waisman, Y. Tanriver, and A. Diefenbach. 2013. A T-bet gradient controls the fate and function of CCR6⁻RORγt⁺ innate lymphoid cells. *Nature.* 494:261–265. http://dx.doi.org/10.1038/nature11813

Matthews, J.R., O.J. Sansom, and A.R. Clarke. 2011. Absolute requirement for STAT3 function in small-intestine crypt stem cell survival. *Cell Death Differ.* 18:1934–1943. http://dx.doi.org/10.1038/cdd.2011.77

Miyoshi, H., R. Ajima, C.T. Luo, T.P. Yamaguchi, and T.S. Stappenbeck. 2012. Wnt5a potentiates TGF-β signaling to promote colonic crypt regeneration after tissue injury. *Science.* 338:108–113. http://dx.doi.org/10.1126/science.1223821

Peterson, L.W., and D. Artis. 2014. Intestinal epithelial cells: regulators of barrier function and immune homeostasis. *Nat. Rev. Immunol.* 14:141–153. http://dx.doi.org/10.1038/nri3608

Pickert, G., C. Neufert, M. Leppkes, Y. Zheng, N. Wittkopf, M. Warntjen, H.A. Lehr, S. Hirth, B. Weigmann, S. Wirtz, et al. 2009. STAT3 links IL-22 signaling in intestinal epithelial cells to mucosal wound healing. *J. Exp. Med.* 206:1465–1472. http://dx.doi.org/10.1084/jem.20082683

Potten, C.S. 1990. A comprehensive study of the radiobiological response of the murine (BDF1) small intestine. *Int. J. Radiat. Biol.* 58:925–973. http://dx.doi.org/10.1080/09553009014552281

Potten, C.S., S.E. Al-Barwari, and J. Searle. 1978. Differential radiation response amongst proliferating epithelial cells. *Cell Tissue Kinet.* 11:149–160.

Reddy, P., and J.L.M. Ferrara. 2003. Immunobiology of acute graft-versus-host disease. *Blood Rev.* 17:187–194. http://dx.doi.org/10.1016/S0268-960X(03)00009-2

Reynders, A., N. Yessaad, T.P. Vu Manh, M. Dalod, A. Fenis, C. Aubry, G. Nikitas, B. Escalière, J.C. Renauld, O. Dussurget, et al. 2011. Identity, regulation and in vivo function of gut NKp46⁺RORγt⁺ and NKp46⁺RORγt⁻ lymphoid cells. *EMBO J.* 30:2934–2947. http://dx.doi.org/10.1038/emboj.2011.201

Ritsma, L., S.I. Ellenbroek, A. Zomer, H.J. Snippert, F.J. de Sauvage, B.D. Simons, H. Clevers, and J. van Rheenen. 2014. Intestinal crypt homeostasis revealed at single-stem-cell level by in vivo live imaging. *Nature.* 507:362–365. http://dx.doi.org/10.1038/nature12972

Salim, S.Y., and J.D. Söderholm. 2011. Importance of disrupted intestinal barrier in inflammatory bowel diseases. *Inflamm. Bowel Dis.* 17:362–381. http://dx.doi.org/10.1002/ibd.21403

Sato, T., R.G. Vries, H.J. Snippert, M. van de Wetering, N. Barker, D.E. Stange, J.H. van Es, A. Abo, P. Kujala, P.J. Peters, and H. Clevers. 2009. Single Lgr5 stem cells build crypt-villus structures in vitro without a mesenchymal niche. *Nature.* 459:262–265. http://dx.doi.org/10.1038/nature07935

Satoh-Takayama, N., N. Serafini, T. Verrier, A. Rekiki, J.C. Renauld, G. Frankel, and J.P. Di Santo. 2014. The chemokine receptor CXCR6 controls the functional topography of interleukin-22 producing intestinal innate lymphoid cells. *Immunity.* 41:776–788. http://dx.doi.org/10.1016/j.immuni.2014.10.007

Sawa, S., M. Cherrier, M. Lochner, N. Satoh-Takayama, H.J. Fehling, F. Langa, J.P. Di Santo, and G. Eberl. 2010. Lineage relationship analysis of RORγt⁺ innate lymphoid cells. *Science.* 330:665–669. http://dx.doi.org/10.1126/science.1194597

Sonis, S.T. 2004. The pathobiology of mucositis. *Nat. Rev. Cancer.* 4:277–284. http://dx.doi.org/10.1038/nrc1318

Spits, H., and T. Cupedo. 2012. Innate lymphoid cells: emerging insights in development, lineage relationships, and function. *Annu. Rev. Immunol.* 30:647–675. http://dx.doi.org/10.1146/annurev-immunol-020711-075053

Verburg, M., I.B. Renes, D.J. Van Nispen, S. Ferdinandusse, M. Jorritsma, H.A. Büller, A.W.C. Einerhand, and J. Dekker. 2002. Specific responses in rat small intestinal epithelial mRNA expression and protein levels during chemotherapeutic damage and regeneration. *J. Histochem. Cytochem.* 50:1525–1536. http://dx.doi.org/10.1177/002215540205001113

Vereecke, L., R. Beyaert, and G. van Loo. 2011. Enterocyte death and intestinal barrier maintenance in homeostasis and disease. *Trends Mol. Med.* 17:584–593. http://dx.doi.org/10.1016/j.molmed.2011.05.011

Visentin, M., R. Zhao, and I.D. Goldman. 2012. The antifolates. *Hematol. Oncol. Clin. North Am.* 26:629–648: ix (ix.). http://dx.doi.org/10.1016/j.hoc.2012.02.002